



Phyllite/bentonite mixture—an alternative effective buffer material for a geological disposal of radioactive waste

Joanna Kyzioł-Komosińska¹ · Janusz Janeczek² · Agnieszka Dzieniszewska¹ · Monika J. Fabiańska² · Aniela Matuszewska² · Ewa Teper² · Ewa Szram² · Tomasz Krzykawski² · Magdalena Pająk¹ · Justyna Czupioł¹

Received: 14 March 2023 / Accepted: 14 November 2023 / Published online: 8 December 2023
© The Author(s) 2023

Abstract

The use of phyllite (Phy) instead of quartz in mixtures with bentonite (B) is recommended as a buffer material for engineering barriers in a geological repository of nuclear waste. The recommendation is based on experimentally determined sorption properties of various Phy/B mixtures. The adsorption capacity of Phy/B mixtures (Phy/B: 75/25, 50/50, and 25/75), the removal efficacy of Eu(III) ions (an analog for fissionogenic lanthanides and actinides), and the rate of their binding reaction were studied using the batch adsorption equilibrium and kinetic experiments at different Eu(III) initial concentrations, solution pH, and solution to adsorbent (L/S) ratio. The adsorption capacity of the Phy/B mixtures increased with the increased bentonite content in the mixture depending on the L/S ratio and solution pH. The highest increase in the adsorption capacity of the Phy/B mixtures compared to phyllite was observed for the Phy/B proportions of 25/75 and 50/50. The rate of the Eu(III) adsorption was the best fitted by the pseudo-second-order kinetic model indicating that the adsorption rate was controlled by chemisorption. The Sips model provided the best correlation of the adsorption experimental data, indicative of more than one adsorption site. The results of this study show the advantage of the Phy/B mixtures in immobilizing Eu and certain fission products by combining adsorption properties of the materials.

Keywords Phyllite/bentonite mixtures · Europium(III) ions · Adsorption/desorption · Radioactive waste repository barriers

Responsible Editor: Georg Steinhauser

Highlights

- Eu(III) adsorption on phyllite/bentonite mixtures as a function of pH, solution to rock ratio, and of initial concentration.
- The pseudo-second-order kinetic model as the best fit for all Phy/B mixtures indicating the chemisorption as controlling adsorption rate.
- The Sips isotherm as the best adsorption experimental model suggests more than one adsorption site.
- Very good effect of bentonite on phyllite Eu(III) adsorption capacity for the 50Phy/50B mixture.
- Chemisorption controls adsorption rate of Eu(III) on all Phy/B mixtures.
- Hydrogen bond formation and precipitation of $\text{Eu}(\text{OH})_3$ are predominant mechanisms of Eu binding by phyllite/bentonite mixtures.
- Very good fit of Sips isotherms to experimental data allows estimation of coefficient of determination values.

Extended author information available on the last page of the article

Introduction

One of the specific goals of radioactive waste disposal is to “inhibit, reduce, and delay the migration of radionuclides at any time from the waste to the accessible biosphere” (IAEA Safety Standards 2011). To achieve this goal, the concept of a multibarrier disposal system in an underground (geological) repository has been developed. The system is made up of engineered and geological (host rock) barriers. The engineered barriers comprise the packaging with vitrified high-level nuclear waste (HLNW) or spent nuclear fuel (SNF), the clay barrier (buffer), and the backfill (Kale and Ravi 2021). The long-term safety of a geological repository for nuclear waste relies on the performance of each of these barriers. However, the role of the clay barrier is crucial in the repository safety assessment (e.g., Itälä 2009; Yang et al. 2014). The principal function of a clay barrier material around waste packages is to protect them from the intrusion of groundwater and, if such an event occurred, to prevent or limit the migration of released radionuclides.

One of the possible scenarios considered in the long-term performance assessment of a radioactive waste repository is the release of radionuclides from breached waste containers and their migration into groundwater through the barriers. The distribution and mobility of the released radionuclides are controlled by the adsorption and ion exchangeable properties of the clay barrier and backfill materials. Moreover, adsorption is important in retarding the potential migration of radionuclides to the aquatic systems and biosphere. Understanding the kinetic process and removal efficacy/adsorption capacity is fundamental for the prediction of radionuclide migration in the surroundings of deep geological disposal sites of high-level nuclear wastes. The studies mainly concern the adsorption capacity of radionuclides on pure minerals or their modified forms as well as on composite materials (Bradbury and Baeyens 2005; García et al. 2019; Hanza et al. 2018; Sharma and Tomar 2011; Verma et al. 2019; Virtanen et al. 2018). To design a highly effective geochemical reactive barrier to immobilize radionuclides in a waste repository, different materials must be parallel studied to analyze their adsorption capacity and adsorption kinetics. However, there have been only a few studies on the adsorption kinetics in this respect (e.g., Baumer and Hixon 2018; Wang 2018).

Currently, bentonite or bentonite mixed with quartz sand is considered to be used as a barrier and backfill material in the deep geological repository of HLNW and SNF because of their low permeability, plasticity (ability to swell), very good adsorption/ion exchange properties, and high thermal conductivity (Itälä 2009; Kónya et al. 2005; Pusch 1992, 2006; Sellin and Leupin 2014; Yang et al. 2014). However, bentonites undergo dehydration, mechanical degradation, and structural transformation decreasing their adsorption capacity at a temperature above 100 °C expected at the contact with waste containers, and other rocks of high thermal resistance and high adsorption capacity for radionuclides are being sought (Xiao et al. 2013). Previous studies show that argillaceous phyllites, while less efficient adsorbents than bentonites, have high adsorption capacity for low initial concentrations of actinides ($< 5 \cdot 10^{-5}$ M) and much higher adsorption capacity than quartz, especially at low pH (Kar et al. 2011; Kyzioł-Komosińska et al. 2019a). Moreover, they are thermally stable up to 400 °C. Therefore, argillaceous phyllite can be considered as a component of a mixture with bentonite instead of quartz to take advantage of phyllite adsorption capacity and proper mechanical properties (compensation for volume changes in swelling/shrinking bentonite), particularly at elevated temperatures. Phyllite clays have recently been used as barrier material in municipal waste landfills due to their low permeability (Garzón et al 2016).

The main purpose of this study is to determine the removal efficacy of Eu(III) ions by phyllite/bentonite (Phy/B) mixtures. Europium is an analog for fissionogenic lanthanides and actinides: Am and Cm; present in HLNW and SNF (NRC Regulation Part 63 2016; Sun et al 2020). Various Phy/B proportions were used in the adsorption experiments to determine the most efficacious mixture for immobilization Eu(III) ions. The rate of the Eu(III) ion removal from solution, the adsorption capacity of the Phy/B mixtures, and mechanisms of adsorption were investigated.

Experimental

Adsorbents

Phyllite used in this study was from the Dewon-Pokrzywna phyllite deposit in the northern foothills of the Opava Mountains in the Eastern Polish Sudetes (Sawicka et al. 2018). Bentonite was from the Miocene Kopernica deposit in Slovakia (Górniak et al. 2016). Mineral and chemical compositions together with textural and physical properties of these minerals are given in Kyzioł-Komosińska et al. (2019a). Powdered phyllite (Phy) and bentonite (B), both with particle size $< 10 \mu\text{m}$, were thoroughly mixed in weight proportions of 75/25, 50/50, and 25/75. The properties of phyllite, bentonite, and their mixtures relevant for the evaluation of their adsorption effectiveness are given in Table 1.

Adsorption experiments

The batch equilibration method was applied to examine the adsorption of Eu(III) from $\text{EuCl}_3 \cdot 6\text{H}_2\text{O}$ solution by the Ph/B mixtures under atmospheric pressure and at

Table 1 Physicochemical properties of phyllite (Phy), bentonite (B), and the Phy/B mixtures

	Phy ^a	75Phy/25B ^b	50Phy/50B ^b	25Phy/75B ^b	B ^a
Specific surface area, m ² /g	3.64	18.55	31.24	44.82	58.24
Cation exchange capacity, cmol ₊ /kg	3.55	21.61	42.11	60.44	79.55
pH	6.85	6.87	6.97	7.15	7.41
pH _{pZC}	6.21	6.14	6.08	6.01	5.95

^aKyzioł-Komosińska et al. (2019a)

^bKyzioł-Komosińska et al. (2019b)

room temperature (23 ± 2 °C). Initial Eu(III) concentrations ranged from 0.01 mg/L ($0.658 \cdot 10^{-7}$ M) to ~ 200 mg/L ($\sim 1.316 \cdot 10^{-3}$ M), and solution to adsorbent (L/S) ratio was 100:1 and 500:1. While in most disposal scenarios concentrations of released radionuclides are much lower than considered in this study (in the low ppm to ppb range), the wide range of initial Eu(III) concentrations used in the adsorption experiments allowed for the more precise measurements. Moreover, a high initial Eu(III) concentration may reflect the worst-case scenario of mass radionuclide release from the waste package after some catastrophic event.

Solution initial pH was adjusted to 4.5 and 7.0 by drop-wise addition of appropriate amounts of 0.01 M HCl or 0.01 M NaOH, respectively. The ionic strength was 0.010 M NaCl. The contact time of adsorbents and solutions was 360 min, i.e., more than necessary to achieve equilibrium inferred from the adsorption kinetics determination. The initial (C_0) and equilibrium (C_{eq}) concentrations of Eu(III) in supernatant solutions were measured after centrifugation and filtration either by the ICP-OES or by ICP-MS spectrometry depending on the Eu(III) concentrations. The removal efficacy (RE) of Eu(III) ions was calculated from the equation:

$$RE = \left[\frac{(C_0 - C_{eq})}{C_0} \right] \cdot 100(\%) \quad (1)$$

Results obtained during this study allowed for the determination of the maximum initial concentrations (C_{0max}) for which Eu(III) ions were fully adsorbed, i.e., $RE = 99.9\%$ and $C_{eq} \leq 0.001$ mg/L.

Adsorption capacity (q) was calculated using the equation:

$$q = \frac{(C_0 - C_{eq})V}{m} (\text{mg/g}) \quad (2)$$

where m mineral mass (g); V solution volume (L).

Duplicate samples were measured, and the standard error in the readings was less than 4%.

Two-parameter isotherm models of Freundlich (Freundlich 1906), Langmuir (Langmuir 1916), and Dubinin-Raduskevich (Dubinin 1960) and the three-parameter Sips isotherm model (Sips 1948) were used to estimate maximum adsorption capacity of the Phy/B mixtures and to determine the affinity between Eu(III) ions and adsorption centers in Phy and B and the bond energy (Table S1 in Supporting Information). The isotherm parameters were determined by non-linear regression using algorithms based on the Levenberg–Marquardt method (Statistic ver. 9.0 software). Two non-linear error functions (Foo and Hameed 2010) were examined in addition to the determination coefficient (R^2) for fitting the calculated isotherm to the experimental data

(Table S2 in Supporting Information). The correlation of experimental results to adsorption isotherms can help to understand the adsorption mechanisms and the degree of the heterogeneity of the adsorbent surface.

Adsorption kinetics

To understand adsorption/desorption processes, both thermodynamic equilibrium and kinetics must be considered (Wang 2018). While thermodynamic data provide information only on the final state of a system, the study of kinetics reveals changes in chemical properties in time and is concerned with the rate of these changes (Azizian 2004).

The Phy/B mixtures were used in the batch kinetic experiments. The effect of the contact time was examined within 2.5–1440-min time-frame for C_0 of 10 and 200 mg/L at pH 4.5 and 7.0 for L/S of 100:1. To determine the impact of the L:S on the adsorption rate, tests were carried out for L/S of 100:1 and 500:1 at C_0 of 10 and 200 mg/L, and pH 7.0. Time elapsed to reach equilibrium in the solute-adsorbent system was further considered in the evaluation of the experimental results. Two kinetic-based reactions, i.e., Lagergren pseudo-first order (PFO) (Begg et al. 2018) and pseudo-second order (PSO) (Blanchard et al. 1984; Ho and McKay 1999), were applied to find the rate-determining step (Table S3 in Supporting Information). The kinetic parameters were estimated by non-linear regression. Tran et al. (2017) recommended the use of nonlinear forms of PFO and PSO to describe the kinetics of adsorption. Due to the transformation of nonlinear to linear forms, the units of the Y and X axes were changed. Two non-linear error functions (Table S2 in Supporting Information) were examined in addition to the coefficient (R^2) to evaluate the fit of the equations to the experimental data (Foo and Hameed 2010).

Auxiliary methods: scanning electron microscopy (SEM), attenuated total reflection Fourier transform infrared spectroscopy (ATR-FTIR)

Operating conditions for these methods are given in the Supporting Information.

Results and discussion

Adsorbents properties

The Phy/B mixtures differed significantly in physicochemical properties depending on the B content. The addition of 25% B into the Phy/B mixture caused a

sixfold increase in CEC up to 21.6 cmol_+/kg , i.e., to the value observed for kaolinite (Ma and Eggleton 1999). The CEC increased 12 times to 42.11 cmol_+/kg in mixtures with 50% B. A similar effect of the B content was observed for the mixtures' SSA (Table 1). Values of pH and pH_{PZC} of the Phy/B mixtures suspension increased from 6.87 to 7.15 and from 6.14 to 6.01, respectively, with an increase in B content.

Europium precipitates

Scanning electron microscopy (SEM)/EDS study of bentonite, phyllite, and the Phy/B mixtures (Table S4 in Supporting Information) after adsorption experiments revealed precipitates of the Eu-phase (Fig. 1). Elongated crystals of the Eu-phase were 5 μm long and < 4 μm wide. The rounded edges of those crystals suggest partial dissolution at the crystal-solution boundary layer. From semi-quantitative EDS analyses, the Eu contents in the crystals precipitated on bentonite and phyllite are on average 69.31 and 68.74

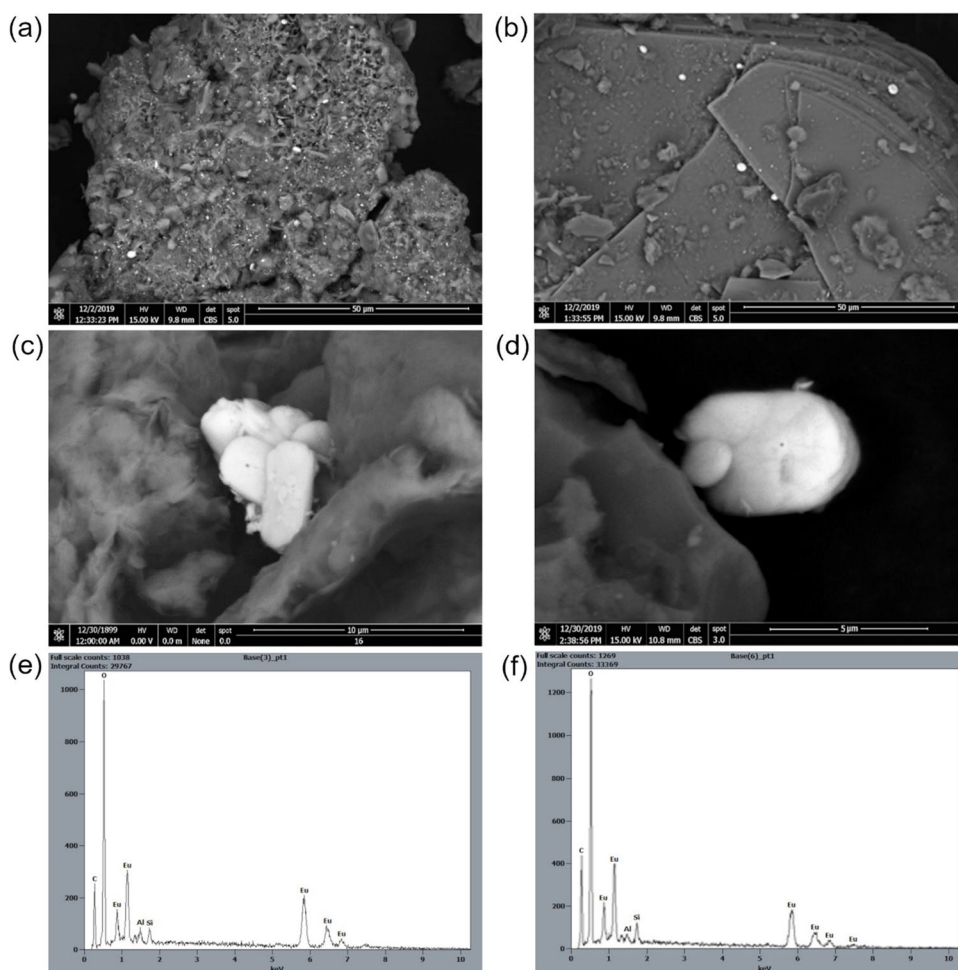
wt.%, respectively. These values are closer to the $\text{Eu}(\text{OH})_3$ stoichiometry (74.86 wt.% Eu) than to Eu_2O_3 (86.36 wt.% Eu) (Table S5 in Supporting Information).

The Eu precipitation was pH-dependent and occurred only at pH 7.0. The bulk contents of Eu adsorbed by montmorillonite in bentonite and by and chloritized biotite in phyllite were about 4.5 and 2.5 wt.%, respectively, regardless of solution pH.

Infrared spectroscopy

Spectra of phyllite collected before and after Eu adsorption are not significantly different. The expected band shifts due to the formation of hydrogen bonds caused by the $\text{Eu}(\text{OH})^{2+}$ bound to $-\text{Al}-\text{OH}$ were not observed in accord with suggestions by Bradbury and Baeyens (2005). The only significant change seen in the IR spectrum of phyllite after the adsorption experiment is the weakening of the 750 cm^{-1} band assigned to the $\text{SiAl}-\text{O}-\text{OH}$ libration of chlorite hydroxyl sites.

Fig. 1 BSE images and EDS spectra of Eu precipitates on: **a** bentonite; **b** biotite partially replaced by Fe-chlorite in phyllite; close-ups (**c**, **d**) show platy crystals of Eu-phase with rounded edges; EDS spectra of the Eu-phase (**e**, **f**). Peaks of Al and Si are from the background minerals and C from the carbon-coating



FT-IR spectra of bentonite after Eu adsorption show more distinct differences compared to phyllite. The 3620 cm^{-1} band is prominent, and its intensity is much higher than neighboring bands. Russell et al. (1970) interpreted the 3624 cm^{-1} montmorillonite band as derived from OH stretching vibrations in Al_2OH and AlMgOH . Bending vibrations of these groups give bands at 915 cm^{-1} (Al_2OH) and much weaker at 843 cm^{-1} (AlMgOH). After Eu adsorption, the intensity of the 915 cm^{-1} band increased slightly, possibly as a result of Eu binding to OH groups. Weakening of bands intensity after Eu adsorption occurred below 900 cm^{-1} , i.e., in the region of OH deformation vibrations in aluminol and

silanol groups (Vaculíková and Plevová 2005). The description of the Phy/B mixture spectra is presented in the Supporting Information.

Adsorption kinetics

Adsorption kinetics was examined for 1400 min; however, the experimental results showed that 180 min was sufficient for reaching an equilibrium state in all Eu-adsorbent systems. There was a rapid and efficient one-step adsorption for C_0 of 10 mg/L, whereas for C_0 of 200 mg/L, a two-step reaction was observed with

Fig. 2 Isothermal ($23 \pm 2\text{ }^\circ\text{C}$) time-dependent Eu(III) adsorption onto Phy/B mixtures for different L/S ratio at solution pH 7.0 (a) and at different initial solution pH for L:S 100:1 (b); exp, experimental data

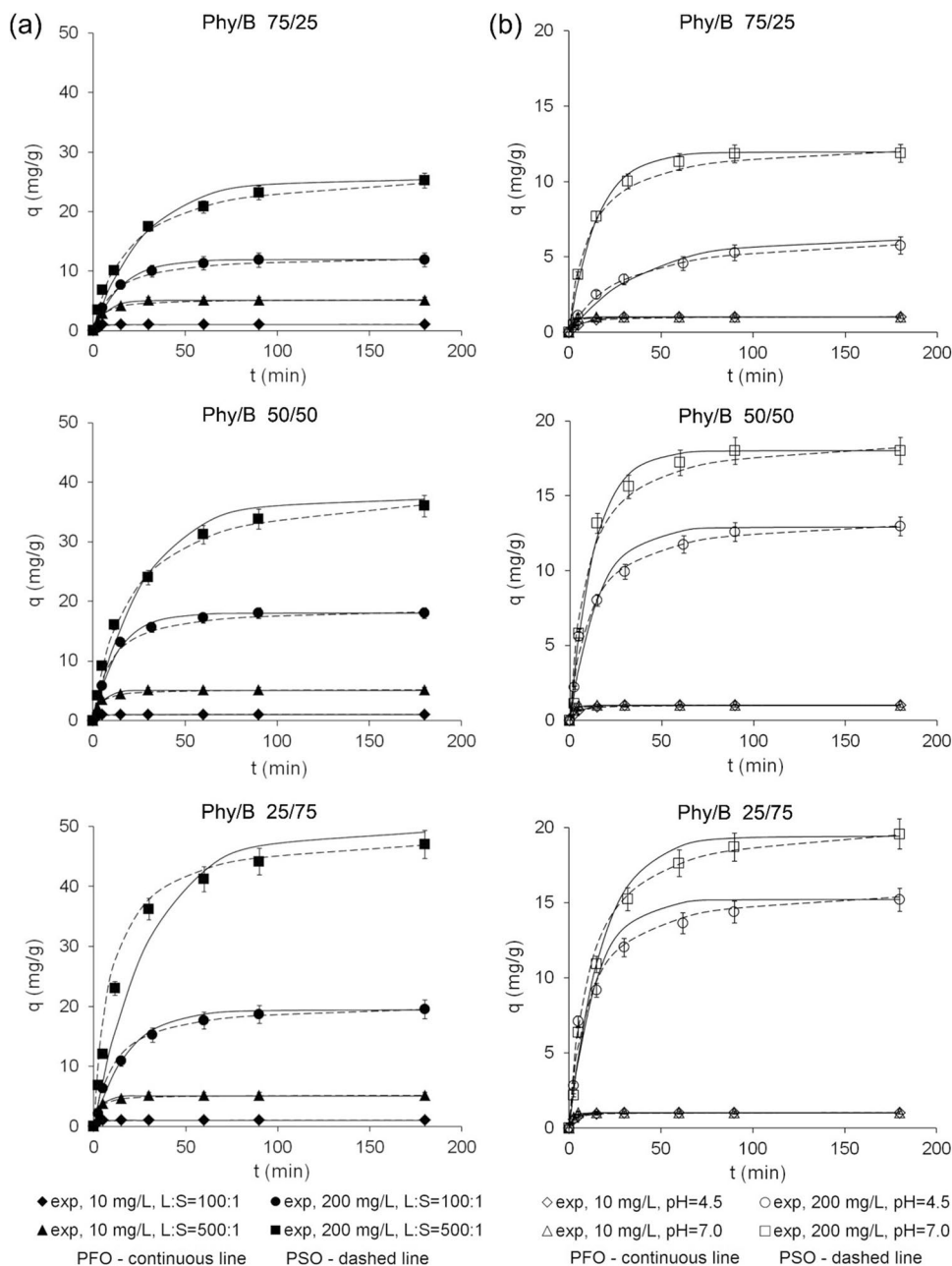


Table 2 Kinetics models fitting parameters for adsorption of Eu(III) ions onto Phy/B mixtures compared to phyllite (Phy) and bentonite (B)

	Phy		Phy/B = 75/25		Phy/B = 50/50		Phy/B = 25/75		B	
	PFO	PSO	PFO	PSO	PFO	PSO	PFO	PSO	PFO	PSO
pH 4.5, C_0 10 mg/L, L:S 100:1										
q	1.011		1.011		1.011		1.011		1.012	
q_e	1.019	1.069	1.009	1.032	1.008	1.047	1.008	1.047	1.01	1.042
k_1, k_2	0.2248	0.3403	0.2064	0.3338	0.2074	0.3416	0.2059	0.3457	0.2029	0.3515
R^2	0.9516	0.9455	0.9985	0.9796	0.9954	0.9879	0.9964	0.9948	0.9899	0.9809
SSE	0.0772	0.1429	0.0080	0.0271	0.0153	0.0138	0.0033	0.0138	0.0093	0.0118
χ^2	0.0291	0.0913	0.0011	0.0293	0.0161	0.0093	0.0031	0.0041	0.0111	0.0137
pH 4.5, C_0 200 mg/L, L:S 100:1										
q	3.50		6.60		13.65		16.80		19.71	
q_e	3.189	3.510	6.1189	6.671	12.91	13.73	15.19	16.81	19.71	21.39
k_1, k_2	0.0532	0.00833	0.0455	0.0074	0.0456	0.0062	0.0416	0.0043	0.0352	0.0016
R^2	0.9485	0.9891	0.9778	0.9975	0.9605	0.9913	0.9456	0.9858	0.9973	0.9869
SSE	0.7471	0.1586	1.435	0.1792	3.453	1.8812	10.02	5.260	1.823	5.580
χ^2	0.3649	0.0926	0.4186	0.0451	1.098	0.2522	0.714	0.794	0.2663	0.3052
pH 7.0, C_0 10 mg/L, L:S 100:1										
q	1.01		1.014		1.014		1.014		1.01	
q_e	1.008	1.042	1.018	1.033	1.019	1.039	1.019	1.034	1.014	1.038
k_1, k_2	0.4837	0.6926	0.4831	0.6865	0.4686	0.6060	0.4396	0.5832	0.3316	0.5801
R^2	0.9889	0.9695	0.9829	0.9763	0.9909	0.9704	0.9912	0.9712	0.9891	0.9632
SSE	0.0124	0.0339	0.0173	0.0442	0.0089	0.0289	0.0086	0.0281	0.0115	0.0386
χ^2	0.0085	0.0205	0.0116	0.0287	0.0065	0.0196	0.0063	0.0319	0.0071	0.0246
pH 7.0, C_0 200 mg/L, L:S 100:1										
q	7.20		12.0		18.07		19.57		20.6	
q_e	7.053	7.741	11.96	12.71	18.03	19.11	19.42	20.60	20.06	21.52
k_1, k_2	0.0561	0.0058	0.0658	0.0055	0.0659	0.0057	0.0676	0.0051	0.0558	0.0039
R^2	0.9949	0.9960	0.9909	0.9701	0.9914	0.9672	0.9923	0.9882	0.9926	0.9902
SSE	0.4169	0.3211	2.248	2.520	6.034	5.358	5.485	4.884	1.0814	4.5168
χ^2	0.2075	0.0891	0.0713	0.2335	0.1288	0.4789	0.6092	0.2332	0.0661	0.2908
pH 7.0, C_0 10 mg/L, L:S 500:1										
q	4.32		5.013		5.013		5.013		5.13	
q_e	4.358	4.891	5.084	5.526	5.083	5.275	5.085	5.233	4.416	5.039
k_1, k_2	0.2433	0.0561	0.2452	0.0553	0.2145	0.0538	0.2151	0.0517	0.2011	0.0485
R^2	0.9929	0.9809	0.9921	0.9861	0.9914	0.9896	0.9923	0.9954	0.9934	0.9968
SSE	0.1184	0.1104	0.2493	0.4404	0.2440	0.2981	0.1998	0.1191	0.5279	0.0851
χ^2	0.0284	0.1524	0.0658	0.0665	0.0561	0.0427	0.0404	0.0194	0.1181	0.0163
pH 7.0, C_0 200 mg/L, L:S 500:1										
Q	22.09		26.4		38.9		48.5		63.84	
q_e	20.08	21.54	25.42	27.39	37.22	40.03	49.18	49.24	61.89	66.11
k_1, k_2	0.0473	0.00325	0.0333	0.0013	0.0362	0.00133	0.0364	0.0013	0.0366	0.00085
R^2	0.9423	0.9879	0.9837	0.9931	0.9933	0.9949	0.9839	0.9541	0.9819	0.9936
SSE	147.6	5.241	9.159	2.906	7.545	1.231	27.25	71.39	42.63	12.67
χ^2	11.73	0.4343	0.3529	0.2445	0.1939	0.1717	0.7941	2.299	0.9813	0.5506

q_e (mg/g) the Eu(III) adsorption at equilibrium, k_1 (1/min) adsorption rate constant for PFO, k_2 (g/mg·min) adsorption rate constant for PSO

initial fast adsorption within 15 min followed by a slower equilibration. At the initial Eu concentration of 10 mg/L, adsorption onto each Phy/B mixture reached equilibrium within 10 min and at the initial Eu concentration of

200 mg/L — within 180 min (Fig. 2). The two-step process is attributed to a fast, diffusion-controlled surface reaction followed by a rate-limiting step that can be explained by a variety of processes including surface precipitation,

diffusion into micropores, structural arrangement, or surface-mediated reduction.

For the PFO and PSO models, the curve fitting parameters (adsorption rate constants, k_1 , and k_2) and the equilibrium adsorbed concentration, q , were calculated (Table 2). High correlation coefficients ($R^2 > 0.95$) were obtained for the non-linear plots of the pseudo-first Lagergren and pseudo-second-order rate equations. Statistical analysis showed that the pseudo-second-order model resulted in better correlations compared to the pseudo-first-order model for C_0 of 200 mg/L and all pH values and L/S ratios. The pseudo-first-order equation fitted well experimental data for C_0 of 200 mg/L for the first 20–30 min of the adsorption process (Fig. 2). According to Ho and McKay (1998), the pseudo-first-order model applies only to a limited fraction of the reaction range. For this reason, the pseudo-second-order model was used to determine the rate constant, k_2 , and the Eu(III) equilibrium adsorbed concentration, q , with respect to C_0 , L/S, and pH. Estimated q was similar to or a little higher than experimentally determined adsorption capacity (Table 2) and depended on the B content in the Phy/B mixtures for C_0 of 200 mg/L. At C_0 of 10 mg/L, the q was constant regardless of the B content in the mixtures (Fig. 2a). A small difference in k_2 determined for various Phy/B mixtures suggests that B content in the mixtures was less important than other experimental conditions. The k_2 strongly depended on the initial Eu(III) concentration, pH, and L/S ratio. It was higher for L:S of 100:1 than for 500:1 for both initial Eu concentrations and all of the Phy/B mixtures. However, the effect of L/S was higher for C_0 of 10 than 200 mg/L (Table 2). The increase in k_2 with increasing content of adsorbents presumably was due to an elevated number of total adsorption sites, including strong adsorption sites in montmorillonite (Bradbury and Baeyens 2002, 2005; Bradbury et al. 2005).

The Eu(III) adsorption rate increased with increasing pH (Fig. 2b) at C_0 of 10 mg/L. This observation can be explained by the mineral surface becoming increasingly negatively charged and, hence, attracting the Eu cations due to electrostatic interactions. There is no correlation between k_2 and pH for C_0 of 200 mg/L, apparently, because the electrostatic interactions had a small share in bonding Eu(III) at the high initial concentration.

The PSO rate constant strongly depended on the initial Eu(III) concentration (Fig. 2a, b). Adsorption rate constant increased with decreasing Eu(III) concentration because there was a larger fraction of binding sites in the adsorbent available for the Eu(III) ions. The higher the initial Eu(III) concentration, the longer it takes to reach equilibrium (Plazinski et al. 2009).

The observed effect of the initial Eu(III) concentration on k_2 was approximately 2 orders of magnitude higher at a lower L/S (Table 2). According to Al-Degs et al. (2006), an inverse relationship between initial Eu(III) concentration and k_2 in adsorption by a natural adsorbent is due to the effect of increased competition for the limited number of active adsorption sites by the adsorbate at higher initial concentrations of heavy metals. The observed decrease in k_2 with increasing Eu(III) concentrations can be explained by the occurrence of strong and weak adsorption sites. At high concentrations, Eu(III) ions tend to preferentially occupy strong binding sites and then weaker ones in clay minerals of the Phy/B mixtures.

The pseudo-second-order kinetic model assumes that the adsorption rate is controlled by chemisorption (He et al 2020), whereas the adsorption capacity is controlled by the number of active adsorption sites (Robati 2013).

Removal efficacy of Eu(III) by the Phy/B mixtures

The maximum initial concentration, C_{0max} , depended on the B content in the Phy/B mixtures (Fig. 3a). The

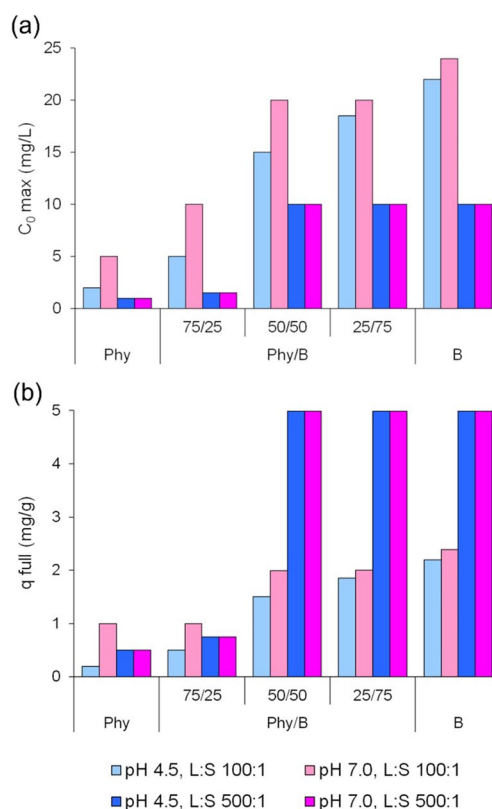
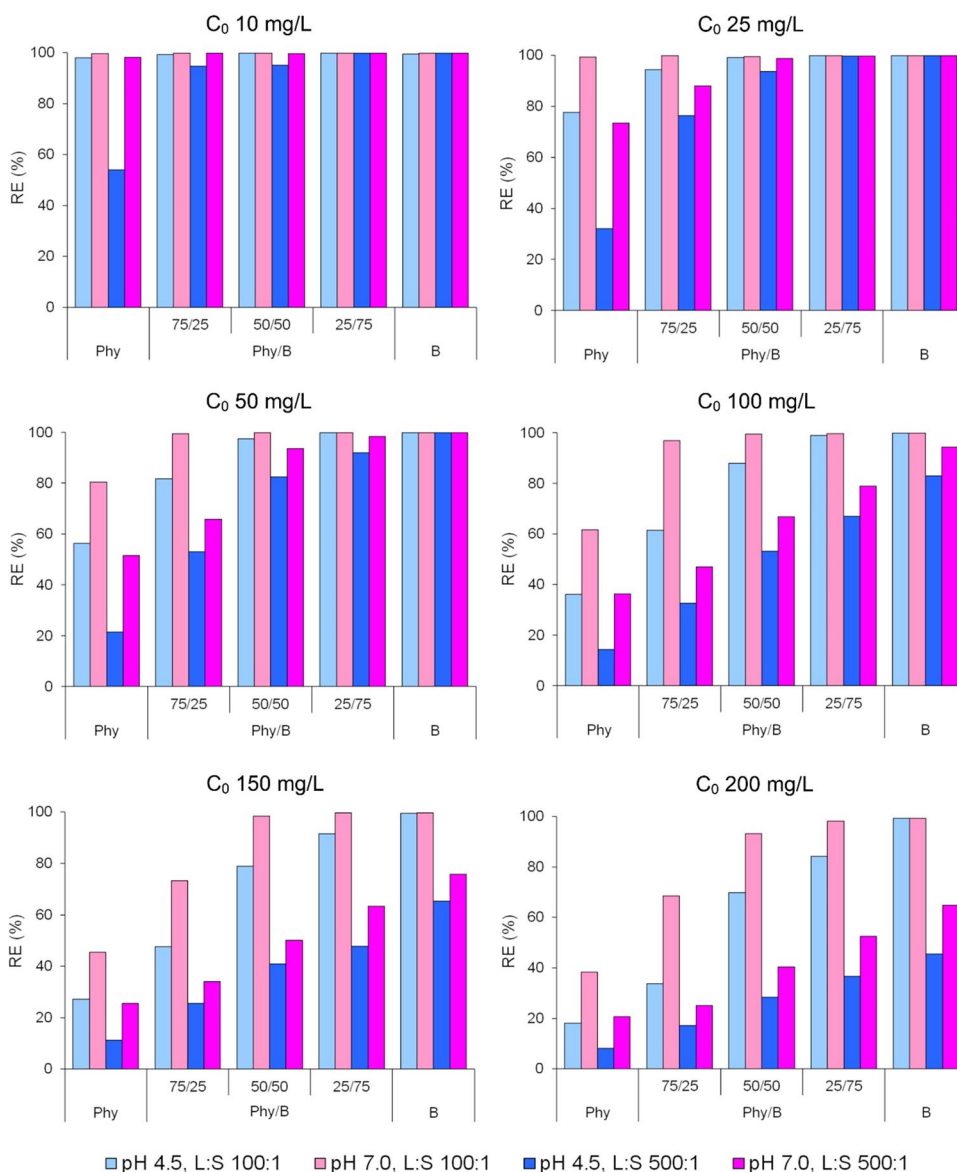


Fig. 3 Maximum initial Eu(III) concentration in solution, C_{0max} (a) and full adsorption of Eu(III) ions by the Phy/B mixtures (b) for the total removal efficacy $RE > 99.99\%$ and $C_{eq} < 0.0001$ mg/L

Fig. 4 Removal efficacy of Eu(III) by the Phy/B mixtures as a function of initial Eu(III) concentrations



highest impact of the B content on C_{0max} was observed for the 50Phy/50B mixture. The highest C_{0max} and the most favorable adsorption conditions were at pH 7 and L:S 100:1. No effect of the initial solution pH on C_{0max} was observed at L:S 500:1. The full adsorption of the 50Phy/50B mixture was close to the full adsorption of B at L:S of 500:1 for both pH values, and it was 0.68 and 0.79 of B adsorption capacity at L:S of 100:1 and pH 4.5 and 7.0, respectively (Fig. 3b).

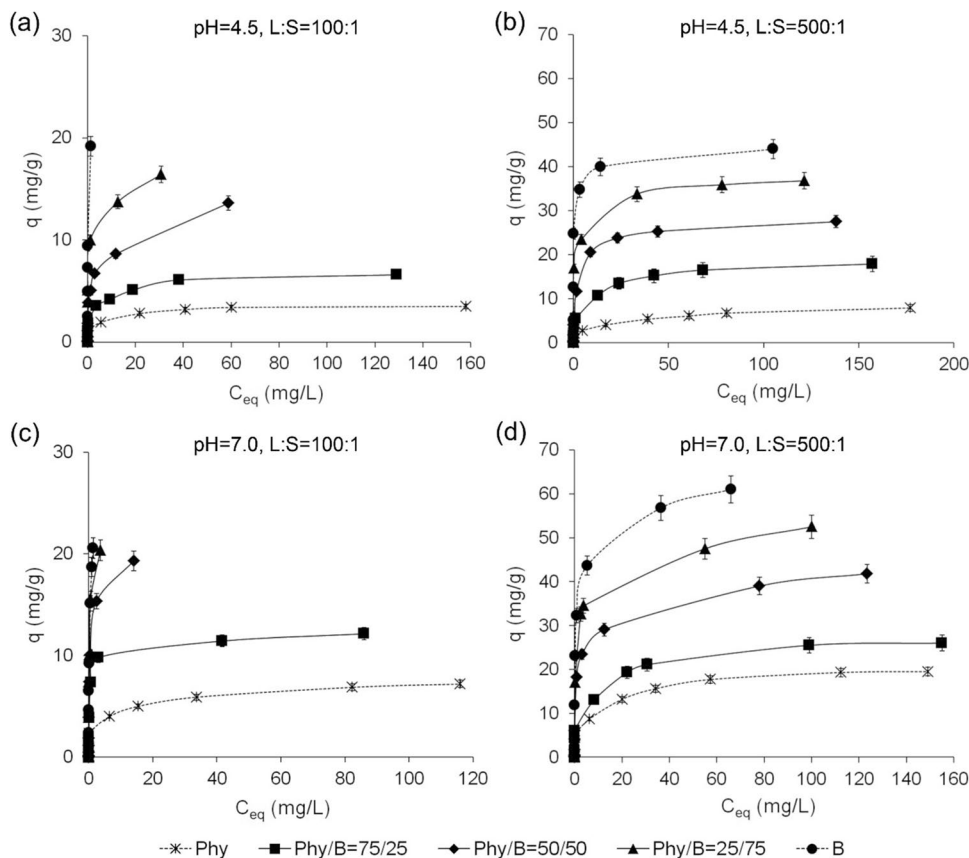
Changes in RE of Eu(III) with increasing Eu(III) initial concentrations ranging from 10 to 200 mg/L were investigated for four pH-L/S systems and six concentrations (Fig. 4). Removal efficacy decreased as the initial Eu

concentration increased, and it depended not only on Phy/B but also on L/S and the initial solution pH.

For the Eu(III) initial concentrations of 10–50 mg/L at pH 7.0 and L/S 100:1, Eu(III) ions were removed from the solution by the adsorption on the Phy/B mixtures as efficiently as on B. A stronger impact of pH and L/S on RE was observed at lower contents of B in the mixtures, whereas a higher impact of L/S than pH was observed in all Phy/B mixtures. The effect of pH was usually higher at L/S 100:1 than at 500:1 (Fig. 4).

Multi-way analysis of variance was used to study the effect of pH, L/S ratio, proportions of Phy to B in the mixtures, and Eu(III) initial concentration on adsorption efficacy of the Phy/B mixtures (Supporting Information).

Fig. 5 The adsorption capacity of the Phy/B mixtures for Eu(III) ions



Adsorption capacity of the Phy/B mixtures and mechanisms of Eu(III) bonding

The adsorption capacity of the Phy/B mixtures for Eu(III) increased with the increase in B content depending on the L/S and pH (Fig. 5). The adsorption system with the highest Eu(III) initial concentration did not reach the complete saturation for the Phy/B mixtures of 50/50 and 25/75 at L/S 100:1, regardless of pH as indicated by the lack of plateau on the adsorption curves (Fig. 5(a, b, c)). The adsorption capacities of the Phy/B mixtures for Eu(III) expressed in cmol_+/ kg ranged from 0.51 to 0.65 of their CECs. High adsorbent concentration at L:S of 100:1 and a high number of total adsorption sites resulted in the partial occupation of the adsorption centers at C_0 of 200 mg/L because of the high cation exchange capacity of montmorillonite in B (Table 1). The 75Phy/25B mixtures adsorbed 6.6 mg/g of Eu(III) at pH 4.5 and 12.14 mg/g at pH 7.0, i.e., 0.60 and 1.1 of CEC, respectively. High concentrations of the Phy/B mixture in solution enhance the possibility of collision between the suspended solid particles of the adsorbents leading to their aggregation. The aggregated particles have lower total surface area which results in a decrease in their adsorption capacity (Yu et al. 2015).

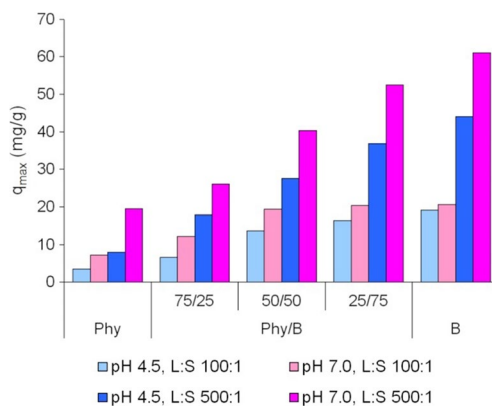


Fig. 6 The maximum adsorption capacity of phyllite, bentonite, and their mixtures

With an increase in the L/S to 500:1, i.e., a decrease in the adsorbent concentration, the adsorption capacity of the Phy/B mixtures for Eu(III) ions increased (Fig. 5(c, d)).

The maximum adsorption capacity of all Phy/B mixtures was higher than their CEC and increased 1.19–1.62-fold at the solution initial pH 4.5 and 1.7–2.4-fold at pH 7.0.

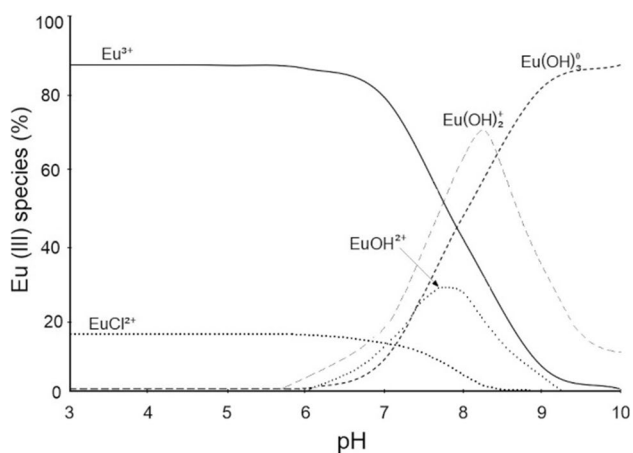


Fig. 7 Distribution of hydrolysed products of Eu(III) at 25 °C in aqueous solution

Therefore, a mechanism other than ion exchange must have been responsible for the Eu-binding.

The adsorption capacity of Phy and Phy/B mixtures was higher at the solution initial pH of 7.0 than 4.5, probably due to the precipitation of $\text{Eu}(\text{OH})_3$ at pH 7.0, both on the surface of Phy/B mixtures and Phy (Fig. 1). The comparison of the maximum adsorption capacity of different Phy/B mixtures reveals the highest increase in adsorption capacity for 75Phy/25B relative to Phy (1.33–2.26-fold increase) and for 50Phy/50B relative to 75Phy/25B (1.53–2.0-fold increase) (Fig. 6).

Speciation of Eu(III), surface properties of the mixtures constituents, and protonation/deprotonation reactions of amphoteric surface functional groups ($\text{Si}-\text{OH}$, Al_2-OH) in clay minerals were all affected by solution pH.

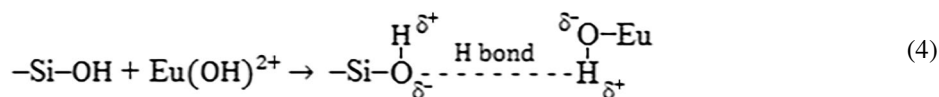
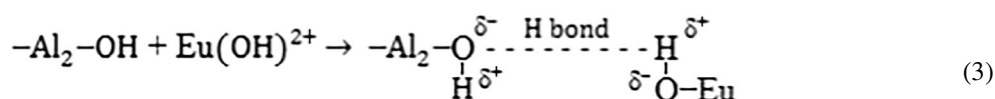
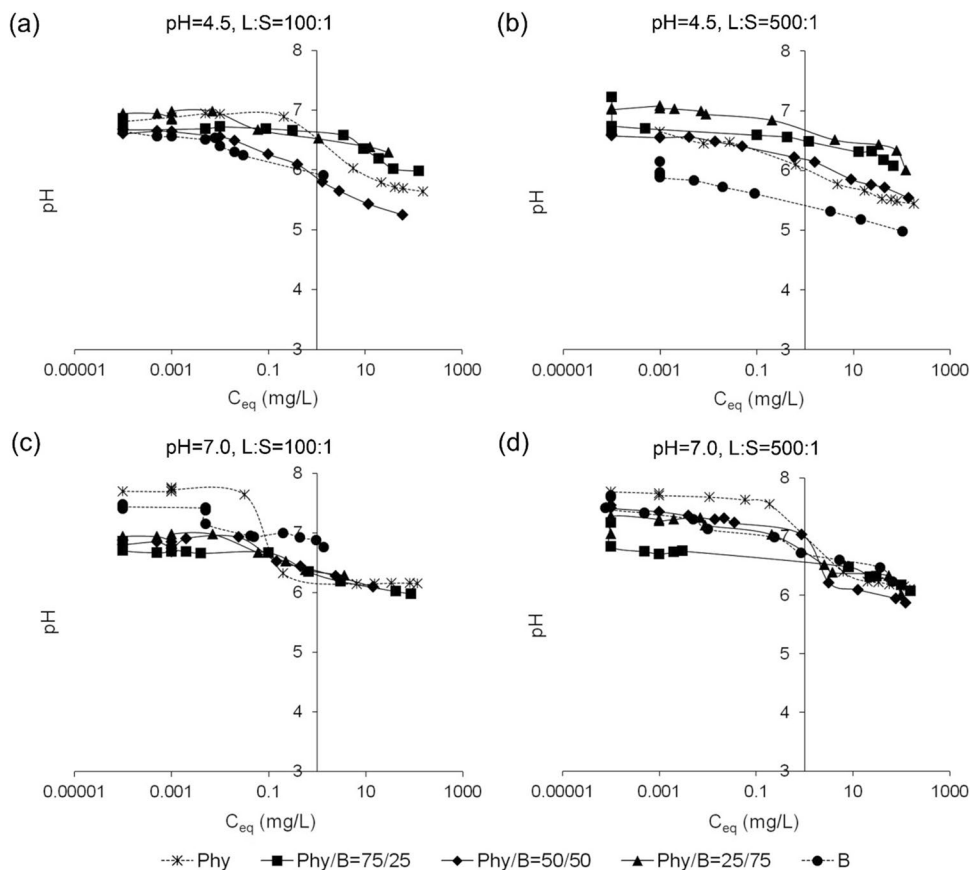


Fig. 8 Changes of pH in equilibrium solutions



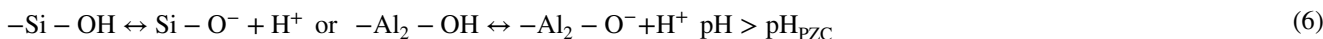
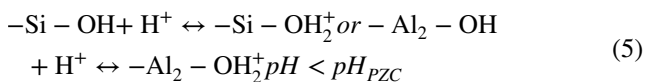
Europium may occur in solution at different valencies: Eu^{3+} and EuCl_2^{2+} at $\text{pH} < 5$ and Eu^{2+} in hydrolyzed species, i.e., $\text{Eu}(\text{OH})_2^{2+}$ and $\text{Eu}(\text{OH})_2^+$ at $\text{pH} > 5.5$ (Fig. 7).

According to Bradbury and Baeyens (2002), hydrolysis of Eu does not occur until $\text{pH} \sim 6$ because of the large Eu ionic radius (0.95 Å). The presence of $\text{Eu}(\text{OH})_2^{2+}$ and $\text{Eu}(\text{OH})_2^+$ ions in solution suggests that they can be bound by hydrogen bonds to the Si–OH and/or $\text{Al}_2\text{–OH}$ surface functional groups of clay minerals in the Phy/B mixtures according to the reactions:

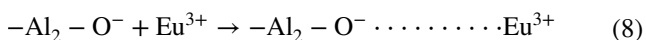
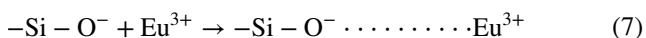
The hydrolyzed species are more hydrophobic than trivalent cations. From the Fig. 7, it can be inferred that $\text{Eu}(\text{OH})_3$ precipitates at $\text{pH} > 6.0$. However, high adsorbent concentration in the solution with the L:S ratio of 100:1 and high initial concentration of Eu(III) (100–200 mg/L) enables precipitation of $\text{Eu}(\text{OH})_3$ even at $\text{pH} \leq 7.0$ as it was the case in this study (Fig. 1).

The equilibrium pH of the Ph/B mixtures suspension decreased as the concentration of Eu(III) in the initial solution increased (Fig. 8) and ranged between 6.89 and 5.25 for L/S 100:1 at initial pH 4.5 and 7.0 and L/S 500:1 at pH 4.5. The equilibrium pH ranged from 7.53 to 5.87 at L/S 500:1 and pH 7.0 (Fig. 8). Equilibrium pH higher than the initial one results in good buffer properties of bentonite and removal of Ca^{2+} and Mg^{2+} ions from montmorillonite (Aitken et al. 1990).

The surface functional groups of minerals are protonated/deprotonated depending on the pH, according to the following equations:



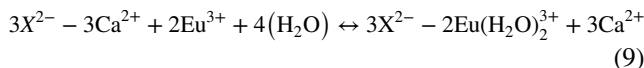
At the initial Eu(III) concentrations between 0.01 and 35 mg/L, the equilibrium solution $\text{pH} > \text{pH}_{\text{PZC}}$ (Table 1), resulting in a negative surface charge of the mixtures-constituting minerals. Europium ions can be electrostatically bound to the negatively charged mineral surfaces according to the reaction:



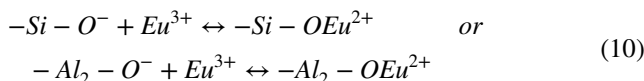
At $C_0 > 35$ mg/L, the surface charge of the Phy/B mixtures was positive due to the protonation reaction of the surface hydroxyl groups; hence, repulsive forces occur between Eu(III) and mineral surfaces.

As a consequence of the layered structure of clay minerals in the Phy/B mixture, Eu(III) ions are adsorbed by:

1. Forming the outer-sphere complexes via cation exchange within the interlayer space in montmorillonite (Liu et al. 2023) and by the attachment to the permanently negatively charged sites on external basal surfaces of montmorillonite at low pH:



2. The formation of the Eu hydroxyl surface inner-sphere complex composed of the cation and silanol (Si–OH) or aluminol ($\text{Al}_2\text{–OH}$) groups at the crystal edges in both bentonite and phyllite:



The inner-sphere complexation at the edges occurs with increased pH (Geckeis et al. 2013).

According to the two-site protolysis non-electrostatic surface complexation and cation exchange (2SPNE SC/CE) model of Bradbury and Baeyens (2002), the Ln/An uptake by montmorillonite can be explained by (i) cation exchange on planar sites, (ii) surface complexation on strong sites ($\equiv\text{S}^{\text{S}}\text{OH}$) with high affinity, but low capacity, and (iii) surface complexation on weak sites ($\equiv\text{S}^{\text{W}1,2}\text{OH}$) with high capacity and low affinity. According to Gao et al. (2021), Am(III) adsorption on Gaomiaozhi bentonite may be described by the surface complexation model including cation exchange species ($(\equiv\text{X})_3\text{Am}$) and three surface complexes ($\equiv\text{S}^{\text{S}}\text{OAm}^{2+}$, $\equiv\text{S}^{\text{S}}\text{OAm}(\text{OH})^+$, and $\equiv\text{S}^{\text{S}}\text{OAm}(\text{OH})_2$). Fernandes et al. (2016) observed that Ln/An³⁺ strong inner-sphere complexes were formed at low loadings through binding to three $\text{Al}(\text{O},\text{OH})_6$ octahedra,

most likely by occupying vacant sites in the octahedral layers of montmorillonite, which are exposed on {010} and {110} edge faces. At higher loadings, Ln/An³⁺ were bonded only via one Al octahedron, forming a weaker, edge-sharing surface complex.

Iron oxyhydroxides in phyllite are additional active centers for the binding of Eu(III).

This study revealed the dependence of the edge site adsorption capacity of the Phy/B mixtures on the surface area. The 25Phy/75B mixture had the highest specific surface area and the highest adsorption capacity. Moreover, adsorption capacity increased with increasing CEC of the Phy/B mixtures. The contribution of individual mechanisms to the binding of Eu(III) by the Phy/B mixtures depends on the amount of bentonite.

Table 3 The isotherm constants for the adsorption of Eu(III) ions onto Phy/B mixtures

	Phy/B					Phy/B				
	100/0	75/25	50/50	25/75	0/100	100/0	75/25	50/50	25/75	0/100
	pH 4.5, L:S 100:1					pH 7.0, L:S 100:1				
Freundlich isotherm										
<i>1/n</i>	0.2127	0.2306	0.2431	0.2705	0.3133	0.2282	0.2476	0.2571	0.2885	0.4141
<i>K_F</i>	1.341	2.389	4.374	7.994	17.97	2.541	5.813	10.61	15.07	17.34
<i>R</i> ²	0.9711	0.9737	0.9877	0.9654	0.9076	0.9848	0.9161	0.9612	0.9608	0.9891
<i>SSE</i>	0.37	1.86	2.03	6.03	19.61	1.38	20.44	12.30	10.49	7.35
χ^2	0.29	1.60	1.78	3.95	7.72	1.85	7.58	3.07	7.01	3.41
Langmuir isotherm										
<i>q</i>	3.50	6.60	13.62	16.42	19.16	7.20	12.14	19.33	20.37	20.56
<i>q_L</i>	3.512	6.649	13.68	16.48	19.80	7.24	12.41	19.38	20.46	21.22
<i>K_L</i>	0.2537	0.3684	0.5203	9.661	27.38	2.821	3.658	3.784	6.315	7.291
<i>R</i> ²	0.9499	0.9635	0.9373	0.9474	0.9884	0.9297	0.9747	0.9674	0.9607	0.9729
<i>SSE</i>	0.77	1.10	1.43	1.49	1.95	6.44	2.49	6.26	10.56	8.35
χ^2	2.71	0.75	7.96	1.27	0.64	2.79	2.14	2.94	3.42	5.10
Dubinin-Raduskevich isotherm										
<i>q_D</i>	0.0400	0.0810	0.1580	0.2010	0.5660	0.0810	0.1331	0.3210	0.4650	0.9980
$\beta \cdot 10^{-3}$	1.677	1.849	1.923	1.409	1.796	1.724	1.299	1.672	1.74	1.807
<i>E</i>	17.26	16.44	16.12	18.84	16.68	17.03	19.62	17.29	16.95	16.63
<i>R</i> ²	0.9890	0.9929	0.9767	0.9838	0.9276	0.9932	0.9633	0.9856	0.9806	0.9909
<i>SSE</i>	0.22	0.51	2.21	3.19	2.87	0.61	2.33	4.90	5.17	3.15
χ^2	0.40	0.46	0.98	2.35	3.73	1.03	2.38	2.88	2.32	2.31
Sips isotherm										
<i>q_S</i>	4.892	8.883	16.67	20.09	31.12	12.67	12.67	23.69	27.23	59.39
<i>K_S</i>	0.4069	0.3816	0.5053	0.9750	1.451	0.2721	1.007	1.168	1.563	0.4178
<i>m_S</i>	0.3869	0.4318	0.3909	0.5867	0.3614	0.3293	0.5262	0.5037	0.5187	0.4996
<i>R</i> ²	0.9909	0.9961	0.9935	0.9853	0.9697	0.9919	0.9946	0.9962	0.9893	0.9902
<i>SSE</i>	0.19	0.27	0.82	1.56	8.30	0.73	0.77	1.83	5.60	4.66
χ^2	0.18	0.28	0.92	1.59	4.32	1.19	1.13	2.30	2.91	2.66
	pH 4.5, L:S 500:1					pH 7.0, L:S 500:1				
Freundlich isotherm										
<i>1/n</i>	0.1964	0.2567	0.3281	0.1991	0.1316	0.1994	0.2059	0.2274	0.2114	0.2183
<i>K_F</i>	0.4725	5.3825	8.977	15.37	25.47	0.5155	9.671	14.776	21.07	26.13
<i>R</i> ²	0.9299	0.9807	0.9807	0.9664	0.9013	0.9441	0.9739	0.9659	0.9645	0.9219
<i>SSE</i>	0.0974	6.46	11.72	12.49	293.6	0.1014	5.38	7.56	12.24	156.3
χ^2	0.163	5.31	3.11	4.02	1.63	0.1823	6.15	5.40	3.65	1.93
Langmuir isotherm										
<i>q</i>	7.90	17.9	27.5	36.8	44.00	19.5	26.00	41.80	52.50	61.0
<i>q_L</i>	7.973	17.95	27.71	37.15	40.47	20.56	27.70	42.33	53.26	61.45
<i>K_L</i>	0.084	0.2958	0.4557	0.537	21.18	0.1089	0.1060	0.6917	1.129	1.587
<i>R₂</i>	0.9366	0.9711	0.9870	0.9624	0.9815	0.9488	0.9611	0.9617	0.9629	0.9482
<i>SSE</i>	4.74	1.09	2.19	2.70	31.96	2.347	1.88	2.65	2.88	143.8
χ^2	0.304	1.64	2.67	3.71	1.24	0.0126	1.23	2.80	2.87	1.559
Dubinin-Raduskevich isotherm										
<i>q_D</i>	0.1030	0.237	0.351	0.391	0.4110	0.2470	0.258	0.481	0.586	0.7090
$\beta \cdot 10^{-3}$	1.361	1.934	1.923	1.408	1.231	2.11	1.472	1.76	1.541	1.562
<i>E</i>	14.05	16.07	16.12	18.44	20.18	15.31	18.43	16.83	18.03	17.92
<i>R</i> ²	0.9909	0.9935	0.9767	0.9829	0.9879	0.9844	0.9705	0.9891	0.9851	0.9820
<i>SSE</i>	0.676	1.67	2.14	4.43	13.26	0.545	1.54	2.70	3.53	34.06
χ^2	0.054	0.872	1.23	2.44	0.634	0.231	1.11	1.13	1.79	0.543

Table 3 (continued)

	Phy/B					Phy/B				
	100/0	75/25	50/50	25/75	0/100	100/0	75/25	50/50	25/75	0/100
Sips isotherm										
q_s	10.76	23.68	30.39	41.25	45.21	25.79	37.15	49.21	58.14	77.56
K_s	0.0631	0.2603	0.4561	0.8075	18.99	0.1961	0.2877	0.5274	0.9594	0.6555
m_s	0.3307	0.5017	0.6408	0.4226	0.8174	0.3785	0.4612	0.4613	0.4722	0.4047
R^2	0.9928	0.9973	0.9931	0.9881	0.9811	0.9944	0.9748	0.9947	0.9967	0.9865
SSE	1.87	0.68	1.48	1.09	1.957	0.466	1.51	1.88	4.16	0.4614
χ^2	0.154	0.452	0.841	0.772	0.233	0.152	0.57	1.23	1.81	0.0629

K_F ((mg/g)·(L/mg)^{1/n}); q_L (mg/g); K_L (L/mg); q_D (mmol/g); β (mol²/J²); E (kJ/mol); q_s (mg/g); K_s (L/mg)^m

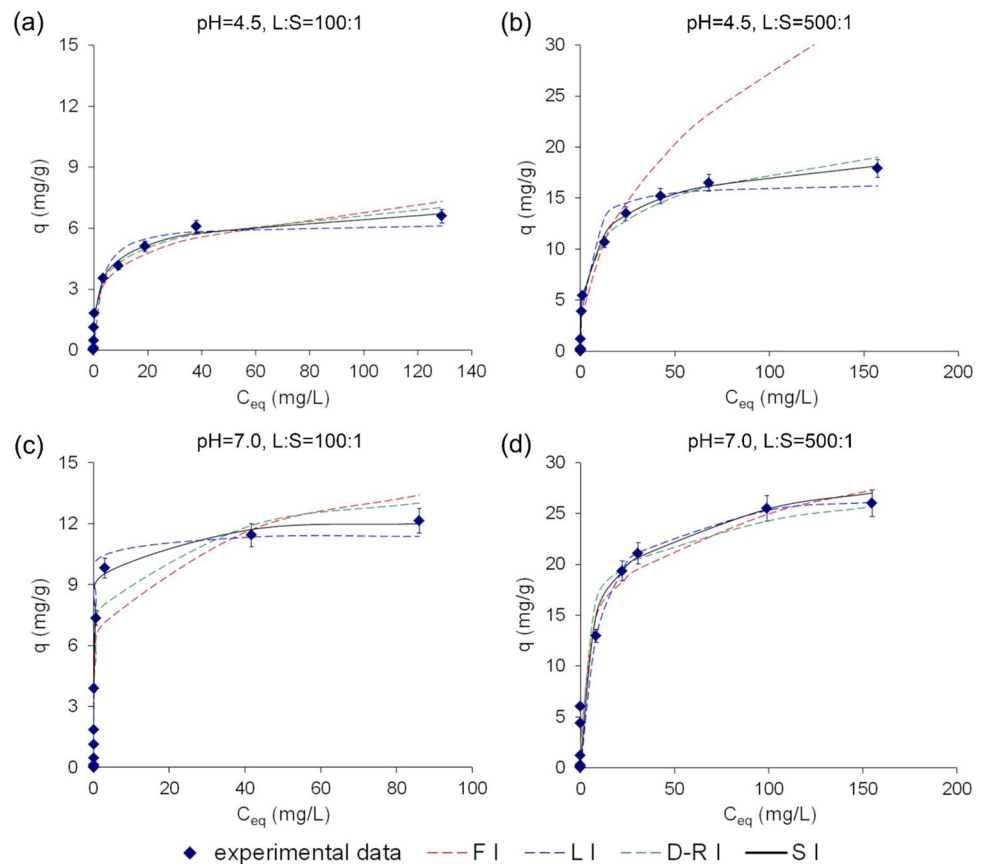
Adsorption isotherms

The parameters of isotherm models determined by the non-linear regression analysis, values of determination coefficient, and non-linear error functions are summarized in Table 3, and the fits of experimental data with four models are shown in Fig. 9.

The isotherm equations described the Eu(III) adsorption on the Phy/B mixtures very well, as suggested by the regression coefficients (R^2) ranging from 0.9161 to 0.9877 for the Freundlich model and from 0.9748 to 0.9962 for the Sips model (Table 3). Values of $1/n$ estimated from the

Freundlich isotherm (Eq. (S1) — Table S1) were below 1 (0.1991–0.3281) and did not depend on experimental conditions. They were indicative of chemical adsorption of Eu(III) ions on all mixtures. The good adsorption capacity of the Phy/B mixtures was indicated by $n > 2$. Values of K_F were higher for mixtures with a high content of bentonite and indicated a higher adsorption intensity at pH 7.0 and L/S 500:1 than at pH 4.5 and L/S 100:1. The fitting of adsorption data to the Freundlich isotherm assumes surface heterogeneity and confirms the high porosity of the Phy/B mixture suggested by the heterogeneous adsorption not limited to the monolayer adsorption (Sharma and Tomar 2011).

Fig. 9 Experimental data and predicted adsorption isotherms of Eu(III) for the Phy/B mixture of 75/25



Results of the error analysis showed that the Langmuir model better simulated the adsorption isotherms than the Freundlich model (Table 3) (He et al 2020). The Langmuir constant, K_L (Eq. (S2) — Table S1) varied depending on the adsorbent surface chemical composition and experimental conditions and was higher for the Phy/B mixture of 25/75 than 75/25. In addition, the effect of the experimental conditions on the affinity of the Phy/B mixture surface for Eu(III) and the bonding energy was similar to that of the K_F values, i.e., it increased with the increase in pH and L:S. The values of the maximum adsorption capacity (q_L) were close to or higher than the theoretical (q_{max}) values for all Eu(III)–Phy/B mixture systems. This observation suggests a monolayer Eu(III) adsorption model associated with ion exchange, in accord with previously obtained results for minerals used for Eu(III) removal from solutions (Hu et al 2010; Kautenburger and Beck 2010; Songsheng et al 2012).

Mean free energy values, E (Eq. (S4)—Table S1), for the Dubinin-Radushkevich isotherm was above 16 kJ/mol ranging from 16.07 to 19.62 kJ/mol as a result of a strong covalent interaction between Eu(III) and the silanol –Si–OH or aluminol –Al–OH groups on bentonite and phyllite surfaces.

The Sips model is a combination of two other models and represents systems in which one adsorbed molecule can occupy more than one adsorption site (Eq. (S5) — Table S1). The Sips model improved the fit of experimental data in the zone of higher curvature of the adsorption isotherms (Fig. 9). Using a third parameter, it logically improves the quality of the mathematical fit. The maximum adsorption capacity values (q_s) for Eu(III) bonding obtained from the Sips model were higher than those derived from the Langmuir isotherm and than the experimentally determined. The parameter K_S changed in the same manner as the constants K_L of the Langmuir model. Differences between experimental and calculated values of adsorption capacity using the Langmuir and Freundlich models showed that at the lower initial concentration, the Freundlich model was a better choice for the characterization of adsorption but at higher initial concentrations; adsorption followed the Langmuir model.

The initial slope of the adsorption isotherm curve provides important information. A curve with a steep initial

slope indicates that the adsorbent has a high affinity for Eu(III), and experimental conditions are most favorable. This affinity is indicated by the affinity constant derived from the Sips model; the highest affinity constant ($K_S = 1.563$) was obtained for the adsorption of Eu(III) on the 25Phy/75B mixture for the L:S 100:1 and pH 7.0.

Distribution coefficient values for Eu(III) adsorbed on Phy/B mixtures

The laboratory batch sorption equilibrium test allowed the estimation of Eu(III) distribution coefficients (K_d). This is an important parameter in transport modelling and one of the key parameters used in the safety analysis of spent fuel repositories (Lehto et al 2019). Distribution coefficients are relevant to the specific geochemical conditions of each system under study and give an indication of the extent of Eu(III) partitioning to the solid phase in different systems and are useful in assessing the migration of Eu(III) in the barrier. It can be defined as the ratio of the solid-phase concentration (q) to the aqueous phase concentration at equilibrium and can be expressed as:

$$K_d = \frac{C_0 - C_{eq}}{C_{eq}} \cdot \frac{V}{m} = \frac{q}{C_{eq}} \quad (11)$$

If the adsorption is described by a non-linear isotherm, the partition coefficient is given by the equation:

$$K_d = \frac{dq}{dC_{eq}} \quad (12)$$

and for the Sips isotherm, which best describes the adsorption of Eu(III) ions by the equation:

$$K_d = \frac{qK_s m C_{eq}^{m-1}}{(1 + K_s C_{eq}^m)^2} \quad (13)$$

The distribution coefficient was calculated for the Phy50/B50 mixture for the following conditions: initial concentration of Eu(III) 0.01–200 mg/L, L/S 100:1 and 500:1, initial concentration of Eu(III) 0.01–200 mg/L, pH 4.5 and 7.0, and is presented in Table 4, and the plots of the $\log K_d$ values for

Table 4 Eu(III) distribution coefficient values (L/g)

Solid phase	L:S 500:1, pH 7.0	L:S 100:1, pH 7.0	L:S 500:1, pH 4.5	L:S 100:1, pH 4.5
Phy	526.1–0.00219	632.8–0.0188	64.22–0.0040	213.3–0.0023
Phy/B 75/25	867.4–0.0039	833.9–0.0427	242.2–0.0110	270.4–0.0055
Phy/B 50/50	1684–0.0261	2117–0.1276	302.88–0.0180	578.1–0.0443
Phy/B 25/75	2811–0.0356	3510–0.7159	1035–0.0153	2175–0.0726
B	3651–0.0694	5633–4.74	1432–0.0836	2929–1.903

the adsorption of Eu(III) on Phy/B of 50/50 against the initial concentration are shown in Fig. 10.

The distribution coefficient values for Eu(III) are strongly dependent on the initial Eu(III) concentration, the pH of the solution, the L/S ratio, and the mineral composition of the solid phase.

The results show that the distribution coefficient values was:

- Higher for bentonite than for phyllite under all conditions and increased with the percentage of bentonite in the mixtures
- Higher for L/S of 100:1 than 500:1 for any initial concentration of Eu(III) ions
- Higher for pH 7.0 than 4.5
- Decreased with increasing initial Eu concentration

The lowest K_d value was observed for Eu(III) adsorption on Phy, and it increased with increasing bentonite in the mixture. Furthermore, as shown in Fig. 10, there were greater differences in K_d values for L/S 500:1 and 100:1 at pH 7.0 than at pH 4.5, and at pH 4.5 and 7.0 for L/S 100:1 than for 500:1. The results for Eu(III) adsorbed on bentonite at L:S 500:1, pH 4.5, and an initial concentration of 40 mg/L indicated that the K_d value was twice as high as the K_d value obtained by Pshinko et al. (2004) for Eu adsorption on Cherkasky montmorillonite under similar conditions.

Conclusions

1. Batch experiments showed a rapid and efficient Eu(III) adsorption on all of the Phy/B mixtures investigated. The adsorption rate constant was strongly dependent on the initial Eu(III) concentration, pH, and L/S ratio. A high correlation of pseudo-second order kinetic model

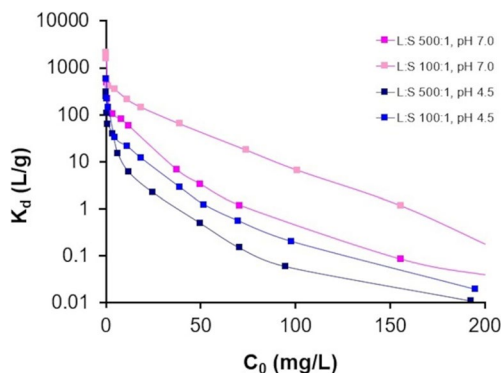


Fig. 10 Distribution coefficient of Eu adsorption on 50Phy/50B mixture

with experimental data showed that the adsorption rate was controlled by chemisorption, while the adsorption capacity was controlled by the number of active adsorption sites.

2. The adsorption capacity of the Phy/B mixtures for Eu(III) increased with the increase of the bentonite content in the Phy/B mixtures, but was dependent on both L/S and solution pH. The addition of bentonite to the mixtures had a strong effect on their CEC and specific surface area.
3. The highest increase in adsorption capacity of Phy/B mixtures compared to phyllite was observed for phyllite/bentonite ratios of 25/75 and 50/50. A greater effect of L/S than of solution pH on both the adsorption capacity and removal efficacy of Eu(III) was observed.
4. Europium can be adsorbed by (i) the outer-sphere complexes via cation exchange in the interlayer space of montmorillonite; (ii) attachment to the permanently negatively charged sites on the outer basal surfaces of montmorillonite; (iii) the inner-sphere complex of the hydroxyl surface composed of the cation and silanol (Si–OH) or aluminol (Al₂–OH) groups at the crystal edges in both bentonite and phyllite; (iv) hydrogen bonding and attraction to a negatively charged mineral surface; and (v) precipitation as Eu(OH)₃.
5. The Sips model showed the best fit to the experimental data, particularly in the zone of higher curvature on the adsorption isotherms indicating that adsorbed Eu(III) can occupy more than one adsorption site.
6. The results of this study show the advantage of the Phy/B mixtures in immobilizing actinides and certain fission products by combining the adsorption properties of montmorillonite and chlorite.

Supplementary Information The online version contains supplementary material available at <https://doi.org/10.1007/s11356-023-31102-6>.

Author contribution All authors contributed to the study conception and design. Material preparation, data collection, and analysis were performed by Joanna Kyzioł-Komosińska, Aniela Matuszewska, Agnieszka Dzieniszewska, Ewa Teper, Justyna Czupiol, and Tomasz Krzykawski. Statistical analyses were performed by Ewa Szram. The first draft of the manuscript was written by Joanna Kyzioł-Komosińska and Janusz Janeczek. Funding acquisition was performed by Monika J. Fabiańska. All authors commented on previous versions of the manuscript. All authors read and approved the final manuscript. Figure preparation Justyna Czupiol and Magdalena Pająk.

Funding The study was supported by National Science Centre project 2014/15/B/ST10/02281 and the statutory fund of the Institute of Environmental Engineering, Polish Academy of Sciences.

Data availability The authors confirm that the data supporting the findings of this study are available within the article and its supplementary materials.

Declarations

Ethical approval Research did not involve human participants and/or animals.

Consent to participate Not applicable.

Consent for publication Not applicable.

Competing interests The authors declare no competing interests.

Open Access This article is licensed under a Creative Commons Attribution 4.0 International License, which permits use, sharing, adaptation, distribution and reproduction in any medium or format, as long as you give appropriate credit to the original author(s) and the source, provide a link to the Creative Commons licence, and indicate if changes were made. The images or other third party material in this article are included in the article's Creative Commons licence, unless indicated otherwise in a credit line to the material. If material is not included in the article's Creative Commons licence and your intended use is not permitted by statutory regulation or exceeds the permitted use, you will need to obtain permission directly from the copyright holder. To view a copy of this licence, visit <http://creativecommons.org/licenses/by/4.0/>.


References

- Aitken R, Moody P, McKinley P (1990) Lime requirement to acidic Queensland soils. I. Relationships between soil properties and pH buffer capacity. *Aust J Soil Res* 28:695–701. <https://doi.org/10.1071/SR9900695>
- Al-Degs YS, El-Barghouthi MI, Issa AA, Khraisheh MA, Walker GM (2006) Sorption of Zn(II), Pb(II), and Co(II) using natural sorbents: equilibrium and kinetics studies. *Water Res* 40:2645–2658. <https://doi.org/10.1016/j.watres.2006.05.018>
- Azzian S (2004) Kinetic models of adsorption: a theoretical analysis. *J Colloid Interface Sci* 276(1):47–52. <https://doi.org/10.1016/j.jcis.2004.03.048>
- Baumer T, Hixon AE (2018) Kinetics of europium sorption to four different aluminum (hydr)oxides: corundum, γ -alumina, bayerite, and gibbsite. *J Environ Radioact* 195:20–25. <https://doi.org/10.1016/j.jenvrad.2018.09.004>
- Begg JD, Edelman C, Zavarin M, Kersting AB (2018) Sorption kinetics of plutonium (V)/(VI) to three montmorillonite clays. *Appl Geochem* 96:131–137. <https://doi.org/10.1016/j.apgeochem.2018.06.001>
- Blanchard G, Maunaye M, Marti G (1984) Removal of heavy metals from waters by means of natural zeolites. *Water Res* 18:1501–1507. [https://doi.org/10.1016/0043-1354\(84\)90124-6](https://doi.org/10.1016/0043-1354(84)90124-6)
- Bradbury MH, Baeyens B (2002) Sorption of Eu on Na- and Ca-montmorillonites: experimental investigations and modelling with cation exchange and surface complexation. *Geochim Cosmochim Acta* 66(13):2325–2334. [https://doi.org/10.1016/S0016-7037\(02\)00841-4](https://doi.org/10.1016/S0016-7037(02)00841-4)
- Bradbury MH, Baeyens B (2005) Modelling the sorption of Mn(II), Co(II), Ni(II), Zn(II), Cd(II), Eu(III), Am(III), Sn(IV), Th(IV), Np(V) and U(VI) on montmorillonite: linear free energy relationships and estimates of surface binding constants for some selected heavy metals and actinides. *Geochim Cosmochim Acta* 69(4):875–892. <https://doi.org/10.1016/j.gca.2004.07.020>
- Bradbury MH, Baeyens B, Geckeis H, Rabung Th (2005) Sorption of Eu(III)/Cm(III) on Ca-montmorillonite and Na-illite. Part 2: surface complexation modeling. *Geochim Cosmochim Acta* 69(23):5403–5412. <https://doi.org/10.1016/j.gca.2005.06.031>
- Dubinín MM (1960) The potential theory of adsorption of gases and vapors for adsorbents with energetically nonuniform surface. *Chem Rev* 60(2):235–241. <https://doi.org/10.1021/cr60204a006>
- Fernandes MM, Scheinost AC, Baeyens B (2016) Sorption of trivalent lanthanides and actinides onto montmorillonite: macroscopic, thermodynamic and structural evidence for ternary hydroxo and carbonato surface complexes on multiple sorption sites. *Water Res* 99:74–82. <https://doi.org/10.1016/j.watres.2016.04.046>
- Foo KY, Hameed BH (2010) Insights into the modeling of adsorption isotherm systems. *Chem Eng J* 156(1):2–10. <https://doi.org/10.1016/j.cej.2009.09.013>
- Freundlich HMF (1906) Over the adsorption in solution. *J Phys Chem* 57:385–471
- Gao P, Zhang D, Jin Q, Chen Z, Wang D, Guo Z, Wu W (2021) Multi-scale study of Am(III) adsorption on Gaomiaozi bentonite: combining experiments, modeling and DFT calculations. *Chem Geol* 581:120414. <https://doi.org/10.1016/j.chemgeo.2021.120414>
- García D, Lützenkirchen J, Petrov V, Siebentritt M, Schild D, Lefevre G, Rabung T, Altmaier M, Kalmykov S, Duro L, Geckeis H (2019) Sorption of Eu(III) on quartz at high salt concentrations. *Colloids Surf A Physicochem Eng Asp* 578:123610. <https://doi.org/10.1016/j.colsurfa.2019.123610>
- Garzón EG, Romero E, Sanchez-Soto PJ (2016) Correlation between chemical and mineralogical characteristics and permeability of phyllite clays using multivariate statistical analysis. *Appl Clay Sci* 129:92–101. <https://doi.org/10.1016/j.clay.2016.05.008>
- Geckeis H, Lützenkirchen J, Polly R, Rabung Th, Schmidt M (2013) Mineral–water interface reactions of actinides. *Chem Rev* 113:1016–1062. <https://doi.org/10.1021/cr300370h>
- Górníak K, Szydlak T, Gaweł A, Klimek A, Tomczyk A, Sulikowski B, Olejniczak Z, Motyka J, Serwicka EM, Bahrnowski K (2016) Commercial bentonite from the Kopernica deposit (Tertiary, Slovakia): a petrographic and mineralogical approach. *Clay Miner* 51(1):97–122. <https://doi.org/10.1180/claymin.2016.051.1.09>
- Hanza MF, Roux JC, Guibal E (2018) Uranium and europium sorption on amidoxime-functionalized magnetic chitosan micro-particles. *Chem Eng J* 344:124–137. <https://doi.org/10.1016/j.cej.2018.03.029>
- He Y, Chen Y-G, Ye W-M, Zhang X-X (2020) Effects of contact time, pH, and temperature on Eu(III) sorption onto MX-80 bentonite. *Chem Phys* 534:110742. <https://doi.org/10.1016/j.chemphys.2020.110742>
- Ho YS, McKay G (1998) Comparison of chemisorption kinetic models applied to pollutant removal on various sorbents. *Process Saf Environ Prot* 76:332–340. <https://doi.org/10.1205/095758298529696>
- Ho YS, McKay G (1999) Pseudo-second order model for sorption processes. *Process Biochem* 34:451–465. [https://doi.org/10.1016/S0032-9592\(98\)00112-5](https://doi.org/10.1016/S0032-9592(98)00112-5)
- Hu J, Xie Z, He B, Sheng GD, Chen L, Li JX, Chen YX, Wang XK (2010) Sorption of Eu(III) on GMZ bentonite in the absence/presence of humic acid studied by batch and XAFS techniques. *Sci China Chem* 53(6):1420–1428. <https://doi.org/10.1007/s11426-010-3064-6>
- IAEA Safety Standards (2011) Disposal of radioactive waste. Specific Safety Requirements No. SSR-5, Vienna
- Itälä A (2009) Chemical evolution of bentonite buffer in a final repository of spent nuclear fuel during the thermal phase. VTT Publications 721. 78 p. Julkaisija – Utgivare – Publisher. Helsinki
- Kale RC, Ravi K (2021) A review on the impact of thermal history on compacted bentonite in the context of nuclear waste management. *Environ Technol Innov* 23:101728. <https://doi.org/10.1016/j.eti.2021.101728>

- Kar AS, Tomar BS, Godbole SV, Manchanda VK (2011) Time resolved fluorescence spectroscopy and modeling of Eu(III) sorption by silica in presence and absence of alpha hydroxy isobutyric acid. *Colloids Surf A Physicochem Eng Asp* 378(1–3):44–49. <https://doi.org/10.1016/j.colsurfa.2011.01.039>
- Kautenburger R, Beck HP (2010) Influence of geochemical parameters on the sorption and desorption behaviour of europium and gadolinium onto kaolinite. *J Environ Monitor* 12:1295–1301. <https://doi.org/10.1039/B914861b>
- Kónya J, Nagy NM, Nemes Z (2005) The effect of mineral composition on the adsorption of cesium ions on geological formations. *J Colloid Interface Sci* 290:350–356. <https://doi.org/10.1016/j.jcis.2005.04.082>
- Kyziół-Komosińska J, Janeczek J, Krzykowski T, Fabiańska MJ, Matuszewska A, Dzieniszewska A, Teper E, Pająk M, Sawicka N (2019) Adsorption of Eu(III) onto bentonite and phyllite: a comparative study. *Appl Clay Sci* 183:105330. <https://doi.org/10.1016/j.clay.2019.105330>
- Kyziół-Komosińska J, Fabiańska MJ, Janeczek J (2019) Sorption and kinetics of Eu(III) on bentonite/phyllite barriers. Challenges in Applied Geology and Geophysics. International Scientific Conference on the occasion of 100th Anniversary of Applied Geology at AGH. 10–13 September. Kraków
- Langmuir I (1916) The constitution and fundamental properties of solids and liquids. Part I. *Solids J Am Chem Soc* 38(11):2221–2295. <https://doi.org/10.1021/ja02268a002>
- Lehto J, Puukko E, Lindberg A, Voutilainen M (2019) Batch sorption experiments of cesium and strontium on crushed rock and biotite for the estimation of distribution coefficients on intact crystalline rock. *Heliyon* 5:e02296. <https://doi.org/10.1016/j.heliyon.2019.e02296>
- Liu H, Fu T, Sarwar MT, Yang H (2023) Recent progress in radionuclides adsorption by bentonite-based materials as ideal adsorbents and buffer/backfill materials. *Appl Clay Sci* 232:106796. <https://doi.org/10.1016/j.clay.2022.106796>
- Ma Ch, Eggleton RA (1999) Cation exchange capacity of kaolinite. *Clay Clay Miner* 47:174–180. <https://doi.org/10.1346/CCMN.1999.0470207>
- NRC Regulation Part 63 (2016) Disposal of high-level radioactive wastes in a geologic repository at Yucca Mountain. Nevada. <http://www.nrc.gov/reading-rm/docollections/cfr/part063/full-text.html>. Accessed 25 May 2016
- Plazinski W, Rudzinski W, Plazinska A (2009) Theoretical models of adsorption kinetics including a surface reaction mechanism: a review. *Adv Colloid Interface Sci* 152:2–13. <https://doi.org/10.1016/j.cis.2009.07.009>
- Pshinko G, Spasenova L, Kornilovich B (2004) Complexation and sorption of europium (III) ions onto clay minerals in the presence of fulvic acids. *Adsorpt Sci Technol* 22:669–678
- Pusch R (1992) Use of bentonite for isolation of radioactive waste products. *Clay Miner* 27(3):353–361. <https://doi.org/10.1180/claymin.1992.027.3.08>
- Pusch R (2006) The performance of clay barriers in repositories for high-level radioactive waste. *Nucl Eng Technol* 38(6):483–488
- Robati D (2013) Pseudo-second-order kinetic equations for modeling adsorption systems for removal of lead ions using multi-walled carbon nanotube. *J Nanostructure Chem* 3(55):1–6. <https://doi.org/10.1186/2193-8865-3-55>
- Russell JD, Farmer VC, Velde B (1970) Replacement of OH by OD in layer silicates and identification of the vibrations of these groups in infrared spectra. *Mineral Mag* 37:869–879. <https://doi.org/10.1180/minmag.1970.037.292.01>
- Sawicka N, Janeczek J, Fabiańska M, Bahranowski K, Krzykowski T, Matuszewska A (2018) Mineralogy and organic geochemistry of phyllite from the Devon-Pokrzywna deposit, the Opava Mountains (SW Poland). *Geol Quarter* 62(4):817–828. <https://doi.org/10.7306/gq.1439>
- Sellin P, Leupin OX (2014) The use of clay as an engineered barrier in radioactive-waste management – a review. *Clay Clay Miner* 61(6):477–498. <https://doi.org/10.1346/CCMN.2013.0610601>
- Sharma P, Tomar R (2011) Sorption behaviour of nanocrystalline MOR type zeolite for Th(IV) and Eu(III) removal from aqueous waste by batch treatment. *J Colloid Interface Sci* 362(1):144–156. <https://doi.org/10.1016/j.jcis.2011.06.030>
- Sips R (1948) On the structure of a catalyst surface. *J Chem Phys* 16:490–495. <https://doi.org/10.1063/1.1746922>
- Songsheng L, Hua X, Mingming W, Xiaoping S, Qiong L (2012) Sorption of Eu(III) onto Gaomiaozi bentonite by batch technique as a function of pH, ionic strength, and humic acid. *J Radioanal Nucl Chem* 292(2):889–895. <https://doi.org/10.1007/s10967-011-1532-x>
- Sun Z, Chen Y-G, Cui Y-J, Ye W-M (2020) Adsorption of Eu(III) onto Gaomiaozi bentonite corroded by cement waters: effect of cement solutions on the long-term sorption performance of bentonite in the repository conditions. *J Clean Prod* 251:119692
- Tran HN, You SJ, Hosseini-Bandegharai A, Chao HP (2017) Mistakes and inconsistencies regarding adsorption of contaminants from aqueous solutions: a critical review. *Water Res* 120:88–116. <https://doi.org/10.1016/j.watres.2017.04.014>
- Vaculíková L, Plevová E (2005) Identification of clay minerals and micas in sedimentary rocks. *Acta Geodynam Geomater* 138:163–175
- Verma PK, Semenikova AS, Krupskaya VV, Zakusin SV, Mohapatra PK, Romanchuk AY, Kalmykov SN (2019) Eu(III) sorption onto various montmorillonites: experiments and modeling. *Appl Clay Sci* 175:22–29. <https://doi.org/10.1016/j.clay.2019.03.001>
- Virtanen S, Meriläinen S, Eibl M, Rabung T, Lehto J, Huitinen H (2018) Sorption competition and kinetics of trivalent cations (Eu, Y and Cm) on corundum ($\alpha\text{-Al}_2\text{O}_3$): a batch sorption and TRLFS study. *Appl Geochemistry* 92:71–81. <https://doi.org/10.1016/j.apgeochem.2018.02.011>
- Wang J (2018) Adsorption of aqueous neodymium, europium, gadolinium, terbium, and yttrium ions onto nZVI-montmorillonite: kinetics, thermodynamic mechanism, and the influence of co-existing ions. *Environ Sci Pollut Res* 25:33521–33537. <https://doi.org/10.1007/s11356-018-3296-0>
- Xiao J, Chen Y, Zhao W, Xu J (2013) Sorption behavior of U (VI) onto Chinese bentonite: effect of pH, ionic strength, temperature and humic acid. *J Mol Liq* 188:178–185. <https://doi.org/10.1016/j.molliq.2013.10.008>
- Yang T, Pusch R, Knutsson S, Xiaodong L (2014) The assessment of clay buffers for isolating highly radioactive waste. *WIT Trans Ecol Environ* 180:403–413. <https://doi.org/10.2495/WM140351>
- Yu S, Mei H, Chen X, Tan X, Ahmad B, Alsaedi A, Hayat T, Wang X (2015) Impact of environmental conditions on the sorption behavior of radionuclide $^{90}\text{Sr(II)}$ on Na-montmorillonite. *J Mol Liq* 203:39–46. <https://doi.org/10.1016/j.molliq.2014.12.041>

Publisher's Note Springer Nature remains neutral with regard to jurisdictional claims in published maps and institutional affiliations.

Authors and Affiliations

Joanna Kyzioł-Komosińska¹ · Janusz Janeczek² · Agnieszka Dzieńszewska¹ · Monika J. Fabiańska²  · Anieli Matuszewska² · Ewa Teper² · Ewa Szram² · Tomasz Krzykowski² · Magdalena Pająk¹ · Justyna Czupioł¹

✉ Monika J. Fabiańska
monika.fabianska@us.edu.pl

² Institute of Earth Sciences, University of Silesia, 60
Będzińska St., 41-200 Sosnowiec, Poland

¹ Institute of Environmental Engineering, Polish Academy
of Sciences, 34 M Skłodowskiej-Curie St., 41-819 Zabrze,
Poland